shown in Fig. 1a, b, corresponding to conditions of zenith angle >110° and <85° respectively. A surprisingly large difference is observed, with discrete aurorae suppressed under sunlit conditions. The difference is especially pronounced in the dusk–midnight sector, where intense discrete aurorae are found to be most common; here the ratio of discrete aurorae under sunlit versus dark conditions is 3.

Because the solar zenith angle at a given local time depends on season and geographical latitude, one would expect to get the same effect by selecting days near the summer and winter solstices, and indeed this occurred in our data set (intense discrete aurorae occur dominantly in the winter bin). But because the effect is about as strong for the full set of data as for those days around solstice we believe it is not a strictly seasonal phenomenon. For either method of event selection, the probability of observing an intense discrete aurora at any one latitudinal cut is about three times that in the favoured conditions (sunlit or summer) than in unfavourable conditions (darkness or winter).

As mentioned above, we wished to investigate the effect of sunlight on aurorae to test the ionospheric conductivity feedback mechanism[3,4]. In this theory, a region of enhanced precipitation becomes a region of enhanced conductivity (because the precipitation ionizes the upper atmosphere), which causes more current to flow between the magnetosphere and ionosphere, further enhancing the precipitation. Such conditions can lead to the type of field-aligned electron acceleration that causes discrete aurorae and is studied here[5]. As originally proposed and considered so far, the role of pre-existing ionospheric conductivity from other sources was not considered. Although an intense arc can indeed generate as much or more conductance than even full sunlight, the ionosphere is primed for the feedback instability only when the background conductivity is low. Under such circumstances any precipitation immediately represents the dominant source of conductance.

To quantify and make explicit the relationship between conductivity and discrete arcs, we calculated the ionospheric conductivity from its main sources, namely sunlight and diffuse aurorae. For sunlight we used an empirical equation relating solar zenith angle to Pedersen conductivity developed by Rasmussen et al.[7]. For calculating the contribution of diffuse electron precipitation we used our own data base of nine years of DMSP satellite observations, with the events of intense field-aligned acceleration removed, along with the equations given by Robinson et al.[8]. The result, calculated under equinox conditions (00 UT on 21 March), is shown in Fig. 2. Superimposed on the conductivity measurements is the well-known statistical location of field-aligned currents out of the ionosphere[9]. Such currents must be complete circuits; they therefore require closure and thus a conducting channel within the ionosphere. Field-aligned currents driven by the magnetosphere out the ionosphere can be supported by ionospheric conductivity from one source or the other except in the dusk–midnight sector. After midnight the conductivity is supported by hot electrons from the Earth's plasma sheet, whose curvature and gradient drift towards dawn places them precisely into the region of upward currents. For this reason, even under winter conditions, the post-midnight sector has fewer aurorae than pre-midnight.

Discrete auroral arcs are impressive displays that have been studied optically for centuries by means up to and including satellite images, although always in darkness. Discrete aurorae can now be understood to be the means whereby the magneto-ionosphere system establishes the conductivity needed to support currents between the magnetosphere and ionosphere. Hot electrons from the nightside plasma sheet combined with sunlight supply conductivity in all local time sectors except from dusk to midnight. Because currents are also required in this region, the mechanism of auroral arcs creates keV-energy electrons from the relatively cold (a few hundred eV) population available, and thereby the necessary conductivity. Indeed, out of 22 mechanisms proposed for creating discrete aurorae[1], only the ionospheric conductivity feedback mechanism explains our result that discrete aurorae are suppressed under sunlit conditions. ☐

1. Borovsky, J. E. J. geophys. Res. **98,** 6101 (1993).
2. Newell, P. T., Lyons, K. M. & Meng, C.-I. J. geophys. Res. **101,** 2599–2614 (1996).
3. Atkinson, G. J. geophys. Res. **75,** 4746–4755 (1970).
4. Sato, T. J. geophys. Res. **83,** 1042–1048 (1978).
5. Lysak, R. J. J. geophys. Res. **96,** 1553–1568 (1991).
6. Evans, D. S. J. geophys. Res. **73,** 2315–2323 (1968).
7. Rasmussen, C. E., Schunk, R. W. & Wickwar, V. B. J. geophys. Res. **93,** 9831–9840 (1988).
8. Robinson, R. M., Vondrak, R. R., Miller, K., Dabbs, T. & Hardy, D. A. J. geophys. Res. **92,** 2565–2569 (1987).
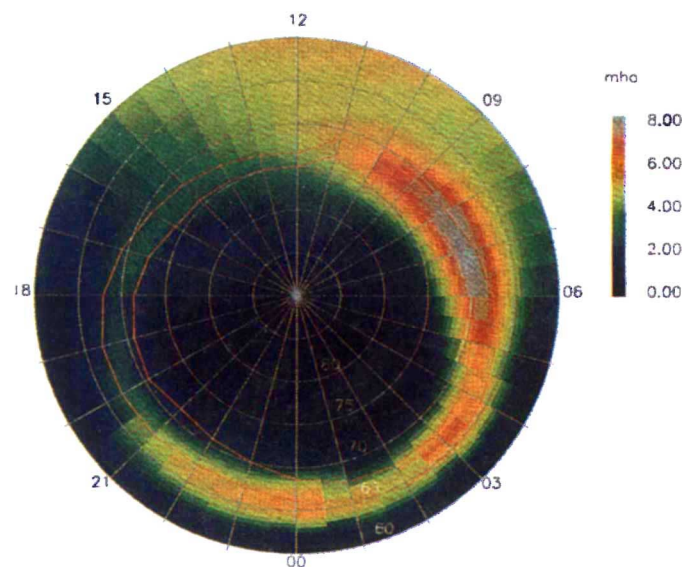9. Iijima, T. & Potemra, T. A. J. geophys. Res. **83,** 599–615 (1978).

FIG. 2 The height-integrated Pedersen conductivity including contributions from diffuse (unaccelerated) aurorae and sunlight at equinox. The red lines give the average position of field-aligned currents out of the ionosphere. Discrete aurorae occur mainly where upward currents are required and conductivity is low.

Turbulent cascades in foreign exchange markets

S. Ghashghaie*, W. Breymann†, J. Peinke‡, P. Talkner§ & Y. Dodge‖

* Fürstensteinerstrasse 4, 4053 Basel, Switzerland
† Institute für Physik der Universität Basel, 4056 Basel, Switzerland
‡ Experimentalphysik II, Universität Bayreuth, 95440 Bayreuth, Germany
§ Paul Scherrer Institut, 5232 Villigen, Switzerland
‖ Groupe de Statistiques, Université de Neuchâtel, 2000 Neuchâtel, Switzerland

THE availability of high-frequency data for financial markets has made it possible to study market dynamics on timescales of less than a day[1]. For foreign exchange (FX) rates Müller et al.[2] have shown that there is a net flow of information from long to short timescales: the behaviour of long-term traders (who watch the markets only from time to time) influences the behaviour of short-term traders (who watch the markets continuously). Motivated by this hierarchical feature, we have studied FX market

dynamics in more detail, and report here an analogy between these dynamics and hydrodynamic turbulence[3-8]. Specifically, the relationship between the probability density of FX price changes (Δx) and the time delay (Δt) (Fig. 1a) is much the same as the relationship between the probability density of the velocity differences (Δv) of two points in a turbulent flow and their spatial separation Δr (Fig. 1b). Guided by this similarity we claim that there is an information cascade in FX market dynamics that corresponds to the energy cascade in hydrodynamic turbulence. On the basis of this analogy we can now rationalize the statistics of FX price differences at different time delays, which is important for, for example, option pricing. The analogy also provides a conceptual framework for understanding the short-term dynamics of speculative markets.

A flow of energy from large to small scales is one of the main characteristics of fully developed homogeneous isotropic turbulence in three spatial dimensions[24]. It provides a mechanism for dissipating large amounts of energy in a viscous fluid. Energy is pumped into the system at large scales of the order of, say, metres (by a moving car or a flying aeroplane) or kilometres (by meteorological events), transferred to smaller scales through a hierarchy of eddies of decreasing sizes, and dissipated at the smallest scale—of the order of millimetres in the above examples. This cascade of kinetic energy extending over several orders of magnitude generates a scaling behaviour of the eddies and manifests itself in a scaling of the moments $\langle (\Delta v)^n \rangle$ of Δv as $(\Delta r)^{\zeta_n}$ (refs 5,6). Here the angle brackets $\langle \rangle$ denote the mean value of the enclosed quantity and Δv is the difference of the velocity component in the direction of the spatial separation of length Δr. Under the assumption that the eddies of each size are space-filling and that the downward energy flow is homogeneous, $\zeta_n = n/3$ (ref. 8). The probability densities $P_{\Delta r}(\Delta v)$ are then scale invariant. This means that if the velocity differences are normalized by their respective standard deviation, the resulting standardized probability densities do not depend on Δr. But for $n > 3$, experimentally determined values of ζ_n follow a concave curve definitely below the ($\zeta_n = n/3$)-line (Fig. 2b). The dependence of the standardized probability density on Δr also provides evidence that eddies of a given size are not space-filling but rather fluctuating in space and time in a typical intermittent way (Fig. 1b).

Our analyses of FX markets are based on a data set provided by Olsen and Associates containing all worldwide 1,472,241 bid–ask quotes for US dollar–German mark exchange rates which have emanated from the interbank Reuters network from 1 October 1992 until 30 September 1993. From these data we have determined the probability densities of price changes $P_{\Delta t}(\Delta x)$ with time delays Δt varying from five minutes up to approximately two days, which are displayed in Fig. 1a. In comparison, Fig. 1b shows the analogous turbulent probability densities $P_{\Delta r}(\Delta v)$, which exhibit the same characteristic features. Using the probability density $P_{\Delta t}(\Delta x)$, the information acquired by observing the market after a time Δt can be quantified as $I(\Delta t) = -\int P_{\Delta t}(\Delta x) \log P_{\Delta t}(\Delta x) \, d(\Delta x)$. It turns out that the dependence of this information on Δt is directly related to the scaling of the variance of Δx with Δt. In turbulence, on the other hand,

the variance of the velocity differences at a distance Δr is proportional to the mean energy which is contained in an eddy of size Δr. This further supports the proposed analogy between energy and information.

Given the analogy between turbulence and FX market dynamics, we expect the moments of FX price changes to scale with the time delay as $\langle (\Delta x)^n \rangle \propto (\Delta t)^{\zeta_n}$. Scaling has already been reported for the mean absolute values of FX returns in ref. 9 and by Evertsz in ref. 1, and for the second moments of the variations of the Standard & Poor's 500 economic index in ref. 10. For FX
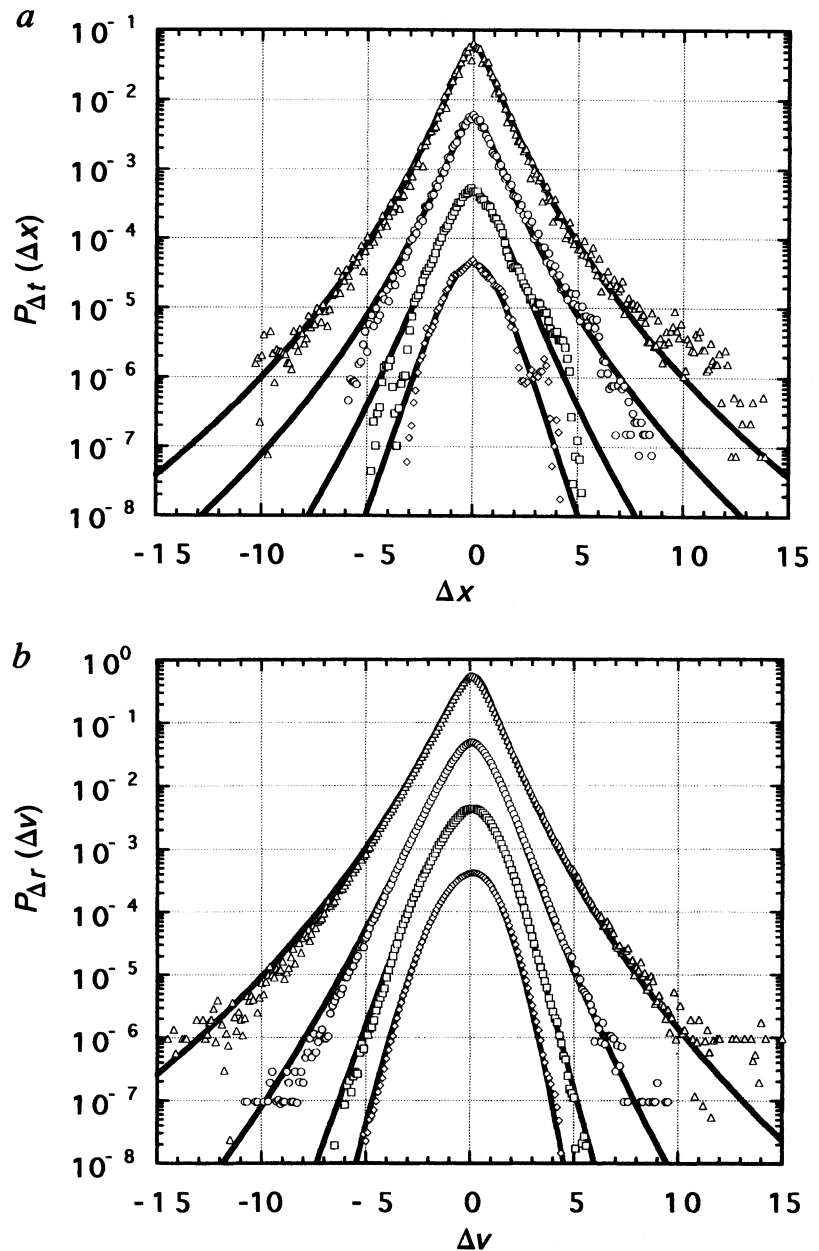

FIG. 1 a, Data points: standardized probability density $P_{\Delta t}(\Delta x)$ of price changes $\Delta x = x(t) - x(t + \Delta t)$ for time delays $\Delta t = 640$ s, 5,120 s, 40,960 s, 163,840 s (from top to bottom). The middle prices $x(t) = (x_{bid}(t) + x_{ask}(t))/2$ have been used (data provided by Olsen & Associates (see text)). The probability density has been calculated in a similar way as ref. 10. Full lines: results of (least-squares) fits carried out according to ref. 7; $\lambda^2 = 0.25$, 0.23, 0.13, 0.06 (from top to bottom). For better visibility, the curves have been vertically shifted with respect to each other. Note the systematic change in shape of the densities. b, Data points: standardized probability density $P_{\Delta v}$ of velocity differences $P_{\Delta r}(\Delta v)$ for a turbulent flow with $\Delta r = 3.3\eta$, 18.5η, 138η, 325η (data taken from ref. 13, $R_\lambda = 598$. Here η is the Kolmogorov scale, where viscous dissipation occurs. Full lines: results of (least-squares) fits carried out according to ref. 7; $\lambda^2 = 0.19, 0.10, 0.04, 0.01$.

market data, it has also been observed that the kurtosis, which is the ratio of the fourth moment and the squared variance, decreases with increasing time delay, that is, the tails of the probability density lose weight[9,11]. Figure 2a shows the higher-order moments of the FX price changes. They scale for time delays Δt varying from about five minutes up to several hours. As in turbulence, the scaling exponents ξ_n depend on the order of the moments in a nonlinear way. Moreover, the ξ_n of the FX data are close to the ζ_n of turbulent data (Fig. 2b). This is also in agreement with the observation that the shapes of the turbulent and FX probability densities, $P_{\Delta r}(\Delta v)$ and $P_{\Delta t}(\Delta x)$, depend on their respective scale parameters in a similar way: both show a decrease of kurtosis with increasing scale parameter[12] (Fig. 1a and 1b).

Even though the probability densities $P_{\Delta t}(\Delta x)$ and $P_{\Delta r}(\Delta v)$ are in principle determined by their moments, this is of little help in practice because errors drastically increase when calculating higher-order moments from observed data. In turbulence, for different experimental situations, the change in shape of $P_{\Delta r}(\Delta v)$ has been successfully parametrized using a method motivated by the energy cascade[7,13,14]. The standardized probability density is approximated by a superposition of gaussian densities with log-normally distributed variances. The variance λ^2 of this log–normal distribution is a measurable form parameter containing information on the energy cascade[15]. It is the only parameter that must be

TABLE 1   Correspondence between fully developed three-dimensional turbulence and FX markets

Hydrodynamic turbulence	FX markets
Energy	Information
Spatial distance	Time delay
Laminar periods interrupted by turbulent bursts (intermittency)	Clusters of low and high volatility
Energy cascade in space hierarchy	Information cascade in time hierarchy
$\langle (\Delta v)^n \rangle \propto (\Delta r)^{\xi_n}$	$\langle (\Delta x)^n \rangle \propto (\Delta t)^{\xi_n}$

adjusted to the data. Applying this method to the FX market data yields a surprisingly good fit (Fig. 1a). Although the data in the centre dominate the fit, the agreement is reasonable also as regards the tails of the probability densities as long as the time delay is shorter than about two days. This is in contrast to fits with Lévy distributions which significantly deviate in the tails[10]. The parameter λ^2, which measures the spread of the variances of the superimposed gaussians (that is, the variance of the log–normal distribution), decreases linearly with $\log \Delta t$ (Fig. 3). This result further confirms the similarity of the statistical behaviour of FX markets with the classical picture of turbulence as given by Kolmogorov[5–7]. In particular, it verifies the scaling of the moments, $\langle (\Delta x)^n \rangle \propto (\Delta t)^{\xi_n}$, in an independent way.

An important aspect of turbulent flows is their intermittent behaviour, that is, the typical occurrence of laminar periods which are interrupted by turbulent bursts. In FX markets this corresponds to clusters of high and low volatility[12], which give rise to relatively high values of the probability densities $P_{\Delta t}(\Delta x)$ both in the centre and the tails. This particular aspect is well reproduced for time delays smaller than two days by the proposed log–normal superpositions of gaussians. However, long interruptions of the trading process (particularly during weekends) affect the probability densities and lead to deviations from the expected shape. Hence, we conclude that the range which is governed by the information cascade has an upper limit. We note that in turbulence also there is an upper length scale, where the energy cascade sets in and beyond which scaling fails.

Different types of models have been proposed to describe the statistical characteristics of price differences of financial indices as, for example, the behaviour of the volatility. Prominent approaches are models using mixtures of distributions[16–18] and ARCH/GARCH-type models[19,20] (see, for example, the overview in ref. 21). But these studies do not address the scaling behaviour of the probability distributions of FX price changes.

It is unlikely that there is a set of a few partial differential equations (like the Navier Stokes equations in hydrodynamics) which might serve as a model of FX market dynamics. More striking is the similarity of the two phenomena, which is accounted for by the existence of a cascade in both cases. This has prompted us to introduce concepts of turbulence in the description of FX
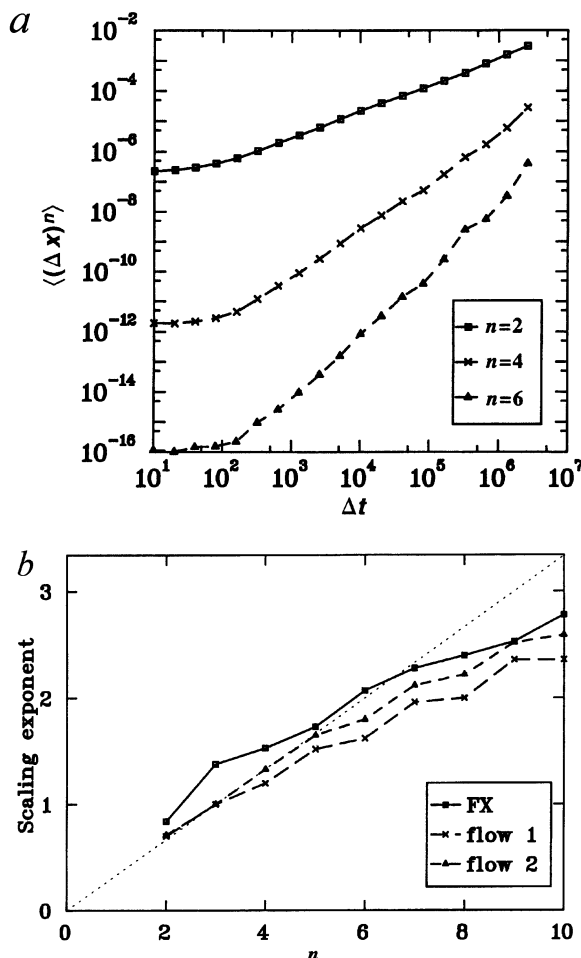

FIG. 2 a, Scaling of moments $\langle (\Delta x)^n \rangle$ with $n = 2, 4$ and 6. b, n-dependence of the scaling factors ξ_n and ζ_n for the nth moments of the probability densities of FX price changes (squares) and hydrodynamic velocity differences taken from ref. 22 (crosses) and ref. 23 (triangles). Note the same qualitative deviation of all curves from a straight line.
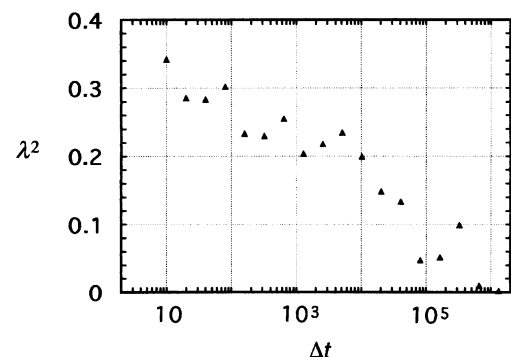

FIG. 3 Dependence of the form parameter λ^2 on Δt (in seconds).

markets, in particular that of an information cascade. Table 1 summarizes the corresponding notions. How far this analogy goes still has to be shown. In any case, we have reason to believe that the qualitative picture of turbulence that has developed during the past 70 years will help our understanding of the apparently remote field of financial markets. □

1. Proc. 1st Int. Conf. on High Frequency Data in Finance (Olsen & Associates, Zürich, 1995).
2. Müller, U. A. et al. J. empirical Fin. (in the press).
3. Landau, L. D. & Lifshitz, E. M. Fluid Mechanics 2nd edn (Pergamon, Oxford, 1987).
4. Monin, A. S. & Yaglom, A. M. Statistical Fluid Mechanics Vols 1 & 2 (ed. Lumely, J.) (MIT Press, Cambridge, MA, 1971 & 1975).
5. Kolmogorov, A. N. J. Fluid Mech. **13**, 82–85 (1962).
6. Obukhov, A. M. J. Fluid Mech. **13**, 77–81 (1962).
7. Castaing, B., Gagne, Y. & Hopfinger, E. Physica D**46**, 177–200 (1990).
8. Kolmogorov, A. N. Dokl. Akad. Nauk. SSSR **30**, 301–305 (1941).
9. Müller, U. A. et al. J. Banking Fin. **14**, 1189–1208 (1990).
10. Mantegna, R. N. & Stanley, H. E. Nature **376**, 46–49 (1995).
11. Baillie, R. T. & Bollerslev, T. J. Business econ. Statist. **7**, 297–305 (1989); Rev. econ. Stud. **58**, 565–585 (1991).
12. Vassilicos, J. C. Nature **374**, 408–409 (1995).
13. Chabaud, B. et al. Phys. Rev. Lett. **73**, 3227–3230 (1994).
14. Peinke, J. et al. in Fractals in the Natural and Applied Sciences Vol. A41, (ed. Novak, M. M.) 295–304 (Elsevier Science Amsterdam, 1994).
15. Naert, A. et al. J. Phys. II Fr. **4**, 215–224 (1994).
16. Granger, C. W. & Orr, D. J. J. Am. statist. Ass. **67**, 275–285 (1972).
17. Clark, P. K. Econometrica **41**, 135–155 (1973).
18. Kon, S. J. J. Fin. **39**, 147–165 (1984).
19. Engle, R. F. Econometrica **50**, 987–1007 (1982).
20. Bollerslev, T., Chous, R. Y. & Kroner, K. F. J. Econometrics **52**, 5–59 (1992).
21. Taylor, S. J. Math. Fin. **4**, 183–204 (1994).
22. Stolovitzky, G., Sreenivasan, K. R. & Juneja, A. Phys. Rev. E**48**, 3217–3220 (1993).
23. Anselmet, F., Gagne, Y., Hopfinger, E. J. & Antonia, R. A. J. Fluid Mech. **140**, 63–89 (1984).
24. Richardson, L. F. Weather Prediction by Numerical Process 66 (Cambridge Univ. Press, 1922).

Identification of a new type of electronic state in the magnetoresistive orthomanganites

J.-S. Zhou, W. Archibald & J. B. Goodenough

Center for Materials Science and Engineering, ETC 9.102, University of Texas at Austin, Austin, Texas 78712-1063, USA

PEROVSKITES of composition $Ln_{1-x}A_xMnO_3$ (where Ln and A are rare-earth and alkaline-earth elements respectively) have become the focus of scientific and technological interest because of their extraordinary electronic and magnetic properties. For example, compositions with $x = 0.3$ exhibit an unusual combination of ferromagnetism and good electrical conductivity[1]; moreover, the observation[2] of a 'colossal' magnetoresistive response near the Curie temperature (T_C), which can be changed dramatically by altering the strength of the Mn–O–Mn interactions[3,15], points to potential practical applications for these materials. Recent resistivity studies[4] of these materials have suggested that the accepted 'tight-binding' band description[5] of the conduction electrons below T_C may be inadequate and that strong interactions between the electrons and dynamic local lattice distortions associated with the Mn sites may be important. Here we report resistivity and thermopower measurements at high pressure, which indicate a more exotic origin for the electronic properties of these materials. We find that below T_C the conduction electrons lose their localized character and condense into extended electronic states that exhibit no energy dispersion. We attribute the formation of this new state to the strong coupling of the conduction electrons to cooperative oxygen vibrations along the Mn–O bond axes.

Hwang et al.[3] increased the strength of the Mn–O–Mn interactions of compounds with $x = 0.3$ (that is, a fixed Mn^{4+}/Mn^{3+} ratio) by decreasing the bond-length mismatch as given by the tolerance factor $t = (R\text{–}O)/\sqrt{2}(Mn\text{–}O)$, where R–O ($R = Ln_{0.7}A_{0.3}$) and Mn–O are the mean equilibrium bond lengths as calculated from room-temperature ionic radii. In the range $0.96 \leqslant t \leqslant 0.97$, Hwang et al.[3] found a first-order transition from polaronic conduction (mobile electronic species 'dressed' in a local lattice deformation) above T_C to a strongly reduced resistivity in the canted-spin ferromagnetic phase below T_C. The canted-spin ferromagnetism can be understood as a competition between antiferromagnetic superexchange interactions via virtual charge transfer between half-filled π-bonding t_2 orbitals on opposite sites of an oxygen atom, that is, $Mn:t_2\text{–}O\text{–}Mn:t_2$ interactions varying as $\cos\theta_{ij}$, and ferromagnetic double-exchange interactions via a rapid (with respect to spin-relaxation time) real charge transfer of σ-bonding e electrons from a high-spin Mn^{3+} to a Mn^{4+} ion, which varies as $\cos(\theta_{ij}/2)$ (ref. 5); θ_{ij} is the angle between spins on neighbouring Mn atoms.

We report an investigation of the compound $(La_{0.25}Nd_{0.75})_{0.7}Ca_{0.3}MnO_3$ that was chosen to have $t \approx 0.96$; at this value of t the colossal magnetoresistance is at a maximum, and the temperature dependence of the resistivity below T_C changes from semiconductive to metallic with increasing t. We have used hydrostatic pressure to increase, at fixed chemical composition, the strength of the Mn–O–Mn interactions from that for $t \approx 0.96$ at ambient pressure.

Figure 1A shows the resistivity ρ versus temperature T, $\rho(T)$, data for several hydrostatic pressures P. We highlight four features: (1) The maximum in the $\rho(T)$ curve occurs at the Curie temperature T_C (ref. 3); the data show a pressure dependence $dT_C/dP > 0$. (2) A strong thermal hysteresis indicates a first-order transition occurs at T_C as previously noted[3]; we plot in Fig. 1B, a thermal hysteresis and T_C for different pressures. (3) Whereas $\rho(T)$ below T_C is commonly reported to be metallic, our compound cannot be a conventional metal at these temperatures for two reasons. First, the dramatic drop in the resistivity on lowering T below T_C does not obey a power law and, second, the magnitude of $\rho(T)$ below T_C, $\rho(30 K)$ for example, decreases by more than three orders of magnitude as the pressure is increased to 15 kbar (Fig. 1B, b). In contrast, the polaronic conductivity at temperatures $T > T_C$ changes by only a factor of two in the same pressure range. Moreover, at lowest temperatures the resistivity increases with decreasing temperature (Fig. 1B, c). (4) The high-pressure limit of the low-temperature resistivity $\rho(0)$ is of the same order as the high-temperature limit of $\rho(T)$.

The conductivity $\sigma = ne\mu$, where n is the density of carriers of charge e with mobility μ, is classified into two regimes: (1) carriers that move diffusively with a mobility $\mu = eD/kT$, where the diffusion coefficient $D = D_0 \exp(-\Delta G_m/kT)$ contains a motional enthalpy ΔH_m in the free energy ΔG_m and (2) itinerant (conduction-band) carriers with an effective mass m^* and a mobility $\mu = e\tau_s/m^*$ that tunnel without activation energy until they are scattered after a mean free time τ_s by a lattice aperiodicity, scattering by acoustic phonons giving $1/\tau_s \propto T$. Neither process has a mobility that is strongly pressure-dependent as can be seen, for example, for the polaronic conduction above T_C in Fig. 1B, a. Therefore, the extremely strong pressure dependence of $\rho(T)$ below T_C is indicative of a sensitive increase in the density of mobile charge carriers with increasing pressure below T_C.

In support of this deduction, we have demonstrated elsewhere[6] that mobile charge carriers are progressively trapped as T is lowered to T_C. In Fig. 1A we plot a Voigt function matched to a $\rho(T)$ curve below T_C. The Voigt function is normally used to